Shen, X., Kind, R., Huang, Z., Yuan, X., Liu, M. (2019): Imaging the Mantle Lithosphere below the China cratons using S-to-p converted waves. - Tectonophysics, 754, 73-79.

https://doi.org/10.1016/j.tecto.2019.02.002

Imaging the Mantle Lithosphere below the China cratons using S-to-p Converted Waves

Xuzhang Shen[a], Rainer Kind[b,c,*], Zhouchuan Huang[d], Xiaohui Yuan[b], Mian Liu[e]

[a] Guangdong Provincial Key Laboratory of Geodynamics and Geohazards, School of Earth Sciences and Engineering, Sun-Yat Sen University, Guanzhou, 510275, China

[b] GFZ German Research Center for Geoscience Telegrafenberg, 14473 Potsdam, Germany (email: kind@gfz-potsdam.de)

[c] Freie Universität Berlin, FR Geophysik, Malteserstr. 74-100, 12249 Berlin, Germany

[d] School of Earth Sciences and Engineering, Nanjing University, Nanjing 210023, China

[e] Dept. of Geological Sciences, University of Missouri, Columbia, MO 65211, USA

[*] corresponding author

Key Words: Thinning of the China cratons, S-to-p converted seismic waves.

Abstract

We used S-to-p converted waves from over a thousand seismic stations of the permanent Chinese National Seismic Network to study the large scale structure of the mantle lithosphere beneath the cratons in China. To avoid possible sidelobes of the Moho caused by the deconvolution in the S-receiver function method, we skipped the deconvolution and used the SV onset time as reference time instead of the time of the deconvolution spike. With this new method the lithosphere- astheno-sphere boundary (LAB) is observed near 80 km depth below both the North and the South China cratons. However, at the north-eastern margin of theTibetan Plateau the LAB is observed at about 160 km depth, smoothly shallowing towards the west and abruptly ending at the western end of the North China Craton. This structure is not visible in traditional S-receiver function data because it is overwhelmed by Moho sidelobes. There is no indication of a deeper (near 200 km) cratonic litho-sphere-asthenosphere boundary in the other parts of the China cratons as it is observed in other cratons. We hypothesise that at the north-eastern margin of the Tibetan Plateau the original thickening of the lithosphere towards the craton is preserved whereas in most parts of the North and South China Cratons the lower part of the lithosphere is removed by some mechanism. The Moho is well observed. It deepens from 30-40 km at the sea shores in the east to 60-70 km below eastern Tibetan Plateau.

1. Introduction

The lithosphere in China has experienced a complex history of amalgamation of Precambrian cratons (the North China Craton, the South China Block and the Tarim Block), the formation of Phanerozoic orogens between them, and the Indo-Asian collision creating the Tibetan Plateau (see e.g. Dong et al., 2012 or Zheng et al., 2013 and references therein and see Fig.1). This history is well studied using geological records of crustal deformation, but what happened in the mantle lithosphere is less clear. An and Shi (2006), based on temperature estimates from the S-velocity model of Huang et al. (2003), determined a westward increase of lithospheric thickness from ~80 km near the coast and below the North China Craton to ~140 km below the Tarim Basin, to ~160 km below the Yangtze Craton and to ~200 km below the Tibetan Plateau. The cratons in eastern China are thinner than most other cratons (e.g. Li et al., 2013a,b; Pandey et al., 2014) and may have been reshaped in the Phanerozoic (Menzies, 2007). The S-receiver function technique is frequently used for detecting the lithosphere-asthenosphere boundary (LAB) and the mid-lithospheric discontinuity (MLD) (see e.g. Kind et al., 2012). It has been applied to data collections along numerous temporary profiles in China. A large number of LAB images using S-receiver functions are produced for the Tibetan Plateau (Kumar et al., 2006; Kind and Yuan, 2010; Zhang et al., 2010; Zhao et al., 2010; Kumar et al., 2013; Xu et al., 2013; Shen et al., 2014, 2015; Ye et al., 2015; Shi et al., 2016). These results show deepening of the Indian LAB to about 200 km underneath the central part of the Tibetan Plateau. There are also several, some less clear, images indicating a southward deepening of the Eurasian LAB below northern Tibet. Feng et al. (2014) observed a south dipping LAB below the north-eastern part of Tibet. Under the North China Craton, Chen et al. (2008, 2014) and Chen (2009) observed the LAB at 60-70 km depth. The shallow LAB in China is in contrast to the deeper (~200 km) LAB found in other cratons (e.g. Fischer et al., 2010; Eaton et al. 2009; Miller and Eaton, 2010; Kind et al. 2013, 2015, 2017, 2019; Sodoudi et al., 2013; Foster et al., 2014; Hansen et al., 2015), also using S-receiver functions.

The S-receiver function method, however, has been questioned by a recent study of Kind et al. (2019). In this study it is shown that the deconvolution technique in the conventional S-receiver function method may cause artificial signals which could be misinterpreted as mid-lithospheric discontinuity (MLD). Kind et al. (2019) used summation of the unfiltered broadband data lined up along the onset times of the S signal on the SV component (named onset method). With this technology the frequently observed MLD in S-receiver functions in the cratonic United States was not confirmed using USArray data, whereas the shallow LAB in the western US was confirmed. This indicates that these apparent MLD observations may have been artifacts due to sidelobes of the Moho signal caused by deconvolution in generating the S-receiver functions. Avoiding these sidelobes also helped to reveal fossil subduction zones below the cratons in the United States. Here we use this new onset method to analyze S-to-p converted signals from a large-scale seismic network of broadband stations in China.

2. Data and Data Processing

The data used in this study have been obtained from the Data Management Center of China National Seismic Network at the Institute of Geophysics, China Earthquake Administration. The China National Seismic Network (CNSN) consists of more than a thousand broadband stations (Zheng et al., 2010). Fig.1 shows the station locations, the Tibetan Plateau and the main cratons in China. All stations belong to 32 sub-networks managed by seismological bureaus of different provinces. The network uses broadband sensors with flat responses to 360, 120 or 60 s. Most stations have sampling rates of 100 Hz. The data are transmitted in real time to the data center in Beijing.

Because the lithosphere of the North China Craton is very thin (near 80 km), the relatively long-period S-receiver function signals from the LAB could interfere with sidelobes from the Moho signal caused by deconvolution. This might not be a large problem in regions where the LAB signal is clearly separated in time from the Moho signal (e.g., Geissler et al., 2010). Several papers have discussed the usage of un-deconvolved traces and of sidelobes due to deconvolution (Kumar et al., 2010; Bodin et al., 2014; Sippl et al., 2017; Li et al., 2007; Kumar et al., 2012; Hansen et al., 2015; Liu and Gao, 2018). Lekic and Fischer (2017) compared different deconvolution methods and illustrated the main limitations of this processing tool. Kind et al. (2019) obtained surprising results with two basic modifications of the S-receiver function method. The first modification is the usage of un-deconvolved and unfiltered broadband traces. The second and decisive modification is the usage of the onset time of the S signal as reference time. The deconvolution method uses the maximum of the deconvolved S signal as reference time and not the onset time.

The first step in the data processing is to rotate the original Z, N, E components into the P, SV, SH (or L, Q, T) system using backazimuth and incidence angles from the US Geological Survey seismological bulletin. Only data from the epicentral distance range of 60 to 85 degrees were used, regardless of the locations of the stations or sources. We automatically picked the first arrival of the SV signal using the algorithm of Baer and Kradolfer (1987) and selected data with a signal-to-noise ratio greater than 4. The sign of the onset was equalised. We also normalised the traces with the absolute maximum within the window of 10 s after the S onset on the SV component. To ensure high-quality data we chose in addition only events for which the amplitudes on the P component are less than 20% of the input SV signal on the SV component within the time window of -50 to -20 s before the S onset. The reason for applying this criterion is that large signals on the P component in that time window can only be noise, perhaps multiple mantle P waves (e.g. Wilson et al. 2006) or S-to-P scattering waves within the crust and lithosphere between the source and the receiver (e.g. Vinnik & Romanowicz 1991). The expected S-to-p converted signal is only a few percent of the incident signal. After applying these data quality criteria we obtained about 65,800 three-component records. To reduce the amount of data we resampled all traces to 10 samples per second. We used the Seismic Handler software package (Stammler 1993; www.seismic-handler.org) to process the data. All the following figures show depth migrated traces. The migration technique has been, for example, described by Kind et al. (2012). Seismic records are back projected along the ray path using the IASP91 global reference model (Kennett and Engdahl, 1991) and summed with some vertical and lateral smoothing. Figs.2,3 show profiles across China computed with the new onset method (A) and for comparison also with the conventional S-receiver function method (B). In Figs.4,5 only the onset method is used. In Fig.2 we marked the seismic signals of the Moho, the lithosphere-asthenosphere boundary (LAB) and the discontinuity at about 410 km depth (410). It should be noted that the depth of all phases should be read at the lower bound of the colored region in the onset method figures and at the central part of the colored region in the deconvolution method figures (marked by black lines in Fig.2A,B). This is due to the different definitions of the reference times.

3. Results along several profiles

In this section we discuss results along several profiles of migrated S-to-p converted waves. Fig. 2 shows two east-west profiles through the North China Craton and the north-eastern edge of Tibetan Plateau. The profiles have different widths marked by the two red lines. The Moho is clearly smoothly deepening from about 40 km depth near the coast to about 60 km depth below the eastern Tibetan Plateau in both methods (Figs.2A,B). The LAB is also clearly visible at about 80 km depth in the east and central North China Craton. At the western end of the North China Craton, the LAB abruptly jumps to about 160 km depth (Figs.2A). Further towards the west the LAB shallows to 110-120 km depth at northeastern Tibet towards the Tarim Basin. This dipping LAB phase is not observed in the result of the deconvolution method (Figs.2B) because it is overwhelmed by sidelobes of the Moho signal. Comparable inclined structures in the upper mantle have also been observed in the United States by the onset method but not by the deconvolution method. Kind et al. (2019) interpreted these features under the US as remains of fossil subductions.

Fig.3 shows two east-west profiles through the South China Craton. The LAB is observed at the same depth like in the North China Craton in Fig.2. However there is no clear signal in this profile like the inclined LAB in the west of the North China Craton. There are some less clear negative signals below eastern Tibet in this profile (question mark in the left panel of Fig.3A) which might indicate a continuation of the inclined LAB observed further north into the South China Craton. Fig.3A (right panel) shows an east-west profile covering the entire South China Craton. It also shows a clear LAB at a depth of ~80 km at its eastern margin reaching to about 115 degrees east. To the west of that longitude it is still visible but much weaker. In Fig.3 are also marked signals from the 410 km discontinuity and a from a velocity decrease just above the 410 km discontinuity marked LVL. In Fig.4 two north-south profiles across the eastern parts of the China cratons are shown, a narrower one parallel to the coast (Fig.4A) and a wider one covering the entire South China Craton (Fig.4B). Both profiles show clearly the LAB near about 80 km depth over the entire profiles. In Fig.4A a north inclined structure marked Y could be the subducting Philippine Sea plate north of Taiwan. We should remember that the inclined incoming rays are also sampling some structure offshore. In the profile through the north-eastern margin of Tibetan Plateau and the western part of the South China Craton (Fig.5A), we do not observe a continuous LAB. In its northern part is a structure marked LAB, which seems to be southward inclined, similar to the structure observed by Feng et al. (2014). It seems to be identical with the eastward inclined LAB structure in Figs.2A. We show in Fig.5B a NW-SE profile, in which the same LAB structure is clearly dipping south-eastward. Besides the marked phases, there are no other significant signals visible. In particular, no deep LAB signals (around 200 km) are observed in almost the entire cratonic China in contrast to some other cratons (e.g. Fischer et al., 2010; Eaton et al. 2009; Miller and Eaton, 2010; Kind et al. 2013, 2015, 2017, 2019; Sodoudi et al., 2013; Foster et al., 2014; Hansen et al., 2015). Under the eastern part of China (Fig.4A), the Moho is at ~30 km depth and the LAB at ~80 km depth. In western part of the China cratons (Fig.5A) the Moho is at a greater depth, near 50 km. These Moho depths are in agreement with the results obtained by He et al. (2014) and Yang et al. (2017) from P-receiver functions. A local exception in the south-western part of the the South China Craton is the shallowing of the Moho to about 30 km depth (Fig.3A, right panel marked Z). This local Moho shallowing is also observed by He et al. (2014) and Yang et al. (2017). There is no large-scale difference in the lithospheric structure between the eastern parts of the North and South China Cratons. Our results confirm earlier results of a thin lithosphere in the North China Craton derived from other techniques (e.g. Chen et al., 2008). The amplitudes of the observed LAB signals vary between 2% and 3% of the incident SV signal. We should point out here again that the traces we are using are amplitude normalised. In the deconvolution technique this is always done by the deconvolution spike. However, in the onset method it is done by the absolute maximum in the window of 10 s after the SV onset which may vary in time from trace to trace. This could make the amplitude observations of the P component less stable. Amplitude information of any S-to-p converted waves should be used carefully since lateral heterogeneities could influence the amplitudes greatly.

4. Discussion and Conclusions

An important result of this research is that there is almost no indication in our data for a negative discontinuity near 200 km depth below the China cratons, which is a feature observed in parts of other cratons and has been explained as cratonic LAB. This result confirms earlier indications of a thin lithosphere below eastern China. For example Feng et al. (2010) observed with surface wave tomography and derived temperatures LAB depths decreasing from west to east beneath the North and South China Cratons. We observed a negative discontinuity at less than 80 km depth under the North China and the South China Cratons. This discontinuity could be considered as the shallow LAB as it is also observed under tectonically active regions, for example in the western United States (e.g. Kind et al., 2019). A similar shallow negative discontinuity, termed MLD, has previously also been observed below the cratonic US using largely the S-receiver function method. However, with our modified method this discontinuity was not confirmed. It may have been caused by sidelobes of the deconvolution. Below the China cratons, however, our new method confirmed and extended earlier observations of the shallow LAB.

Another major structure is a negative discontinuity beneath the north-eastern margin of the Tibetan Plateau dipping from 110-120 km depth to about 160 km depth in south-east direction at the western boundary of the North China Craton. This thick lithospheric region at the edge of the North China Craton could be interpreted as remains of the originally thicker lithosphere of the entire China cratons which lost their lower part.

A more technical conclusion is that the new onset method for treating S-to-p converted waves in the upper mantle leads to new and interesting results. The sidelobes have disappeared in the new method and new structures in the mantle lithosphere become visible which have been overwhelmed by Moho sidelobes contained in the traditional S-receiver function method.

Acknowledgments

Waveform data for this study are provided by the Data Management Centre of the China National Seismic Network at the Institute of Geophysics (SEISDMC, doi10.11998/SeisDmc/SN). This work was supported by the project “SPP 2017 - Mountain Building Processes in 4D” by the Deutsche Forschungsgemeinschaft (DFG). X. Shen acknowledges the National Natural Science Foundation of China (Grant 41574077 and 41730212), National Key Research and Development Program of China (2017YFC1500100), Guangdong Province Introduced R&D Team of Geological Processes and Natural Disasters around the South China Sea (2016ZT06N331).

References

An, M., Shi, Y., 2006. Lithospheric thickness of the Chinese continent. Physics Earth Planet. Int. 159, 257-266.

Baer, M., Kradolfer, U., 1987. An automatic phase picker for local and teleseismic events, Bull. Seismol. Soc. Am., 77(4), 1437–1445.

Bodin, T., Yuan, H.Y., Romanowicz, B., 2014. Inversion of receiver functions without deconvolution-application to the Indian craton. Geophys. J. Int. 2, 1025-1033.

Chen, L., Tao, W., Zhao, L., Zheng, T.Y., 2008. Distinct lateral variation of lithospheric thickness in the northeastern North China Craton. Earth Planet. Sci. Lett. 267, 56–68.

Chen, L., 2009. Lithospheric structure variations between the eastern and central North China Craton from S- and P-receiver function migration. Physics Earth Planet. Int. 173, 216–227.

Chen, L., Jiang, M., Yang, J., Wei, Z., Liu, C., ling, Y., 2014. Presence of an intralithospheric discontinuity in the central and western North China Craton: Implications for destruction of the craton. Geology 42, 3, 223-226.

Dong, S.W., Li, T.D., Lü, Q.T., Gao, R., Yang, J.S., Chen, X.H., Wei, W.B., Zhou, Q., SinoProbe Team, 2013. Progress in deep lithospheric exploration of continental China: A review of SinoProbe. Tectonophysics 606, 1-13.

Eaton, D.W., Darbyshire, F., Evans, R.L., Grütter, H., Jones, A.G., Yuan, X., 2009. The elusive lithosphere–asthenosphere boundary (LAB) beneath cratons. Lithos doi.org/10.1016/j.lithos.2008.05.009.

Fischer, K.M., Ford, H.A., Abt, D.L., Rychert, A.C., 2010. The lithosphere-asthenosphere boundary. Annu. Rev. Earth Planet. Sci. 38, 549–73.

Feng, M.,van der Lee, S.,An, M.,Zhao, Y., 2010. Lithospheric thickness, thinning, subduction, and interaction with the asthenosphere beneath China from the joint inversion of seismic S-wave train fits and Rayleigh-wave dispersion curves. Lithos 120, 116–130.

Feng, M., Kumar, P., Mechie, J., Zhao, W., Kind, R., Su, H., Xue, G., Shi, D., Qian, H., 2014. Structure of the crust and mantle down to 700 km depth beneath the East Qaidam basin and Qilian Shan from P and S receiver functions. Geophys. J. Int. 199, 1416-1429.

Foster, K., Dueker, K., Schmandt, B., Yuan, H., 2014. A sharp cratonic lithosphere-asthenosphere boundary beneath the American Midwest and its relation to mantle flow, Earth Planet. Sci. Lett., 402, 82–89.

Geissler, W.H., Sodoudi, F., Kind, R., 2010. Thickness of eastern and central European lithosphere as seen by S receiver functions. Geophys. J. Int. 181, 604-634.

Huang, Z., Li, H., Zheng, Y., Peng, Y., 2009. The lithosphere of North China craton from surface wave tomography. Earth Planet. Sci. Lett., 288, 164-173, 10.1016/j.epsl.2009.09.019

Huang, Z., Su, W., Peng, Y., Zheng, Y., Li, H., 2003. Rayleigh wave tomography of China and adjacent regions. J. Geophys. Res. 108 (B2), 2073.

Hansen, S.M., Dueker, K., Schmandt, B., 2015. Thermal classification of lithospheric discontinuities beneath USArray. Earth Planet. Sci. Lett. 431: 36-47.

Kennett, B.L.N., Engdahl, E.R., 1991. Travel times for global earthquake location and phase identification. Geophy. J. Int. 105, 429–465.

He, R., Shang, X., Yu, C., Zhang, H., Van der Hilst, R.D., 2014. A unified map of Moho depth and Vp/Vs ratio of continental China by receiver function analysis. Geo-phys. J. Int.199, 1910–1918.

Kind, R., 1985. The reflectivity method for different source and receiver structures and comparison with GRF data. J. Geophys/Z. Geophysik 58,146-152.

Kind, R., Yuan, X., Saul, J., Nelson, D., Sobolev, S.V., Mechie, J., Zhao, W., Kosarev, G., Ni, J., Achauer, U., Jiang, M., 2002. Seismic images of crust and upper mantle beneath Tibet: evidence for Eurasian plate subduction. Science 298, 1219–1221.

Kind, R., Yuan, X.H., 2010. Seismic images of the biggest crash on Earth. Science 329, 1479–1480.

Kind, R., Yuan, X., Kumar, P., 2012. Seismic receiver functions and the lithosphere-asthenosphere boundary. Tectonophysics 536-537, 25-43.

Kind, R., Sodoudi, F., Yuan, X., Shomali, H., Roberts, R., Gee, D., Eken, T., Bianchi, M., Tilmann, F., Balling, N., Jacobsen, B.H., Kumar, P., Geissler, H.W., 2013. Scandinavia: a former Tibet?, Geochem. Geophy. Geosy., 14, 4479–4487.

Kind, R., Yuan, X., Mechie, M., Sodoudi, F., 2015. Structure of the upper mantle in the north-western and central United States from USArray S-receiver functions, Solid Earth, 6, 957–970.

Kind, R., Handy, M.R., Yuan, X., Meier, T., Kämpf, H., Soomro, R., 2017. Detection of a new sub-lithospheric discontinuity in central Europe with S-receiver functions, Tectonophysics, 700, 19-31.

Kind, R., Mooney, W.D., Yuan, X., 2019. New insights into structural elements of the upper mantle beneath the contiguous United States from S-to-p converted waves. J. Geophys. Res., Solid Earth, in review.

Kumar, P., Yuan, X., Kind, R., Ni, J., 2006. Imaging the colliding Indian and Asian lithospheric plates beneath Tibet. J. Geophys. Res. 111, B06308, doi:10.1029/2005JB003930.

Kumar, P., Kind, R., Yuan, X., 2010. Receiver function summation without deconvolution. Geophysical Journal International 180, 1223–1230.

Kumar, P., Kind, R., Yuan, X., Mechie, J., 2012. USArray receiver function images of the lithosphere-asthenosphere boundary. Seismological Research Letters, 83(3), 486–491.

Langston, C.A., 1979. Structure under Mount Rainier, Washington, inferred from teleseismic body waves. J. Geophys. Res. 84 (B9), 4749-4762.

Lekic, V., Fischer, K.M., 2017. Interpreting spatially stacked Sp receiver functions, Geophys. J. Int., 210, 874-886.

Li, X., Yuan, X., Kind, R., 2007. The lithosphere-asthenosphere boundary beneath the western United States, Geophys. J. Int., 170, 700–710, doi:10.1111/j.1365-246X.2007.03428.x.

Li, Y., Wu, Q., Pan, J., Zhang, F., Yu, D., 2013a. An upper-mantle S-wave velocity model for East Asia from Rayleigh wave tomography. Earth Planet. Sci. Lett., 377–378, 367-377.

Li, S.R., Santosh, M., Zhang, H.F., Shen, J.F., Dong, G.C., Wang, J.Z., Zhang, J.Q., 2013b. Inhomogeneous lithospheric thinning in the central North China Craton: zircon U–Pb and S–He–Ar isotopic record from magmatism and metallogeny in the Taihang Mountains. Gondwana Research 23, 141–160.

Liu, L., Gao, S.S., 2018. Lithospheric layering beneath the contiguous United States constrained by S-to-P receiver functions. Earth and Planetary Science Letters 495, 79–86.

Menzies, M., Xu, Y., Zhang, H., Fan, W., 2007. Integration of geology, geophysics and geochemistry: a key to understanding the North China craton. Lithos 96, 1–21.

Miller, M.S., Eaton, D.W., 2010. Formation of cratonic mantle keels by arc accretion: Evidence from S receiver functions. Geophys. Res. Lett. 37, L18305, doi:10.1029/2010GL044366

Nelson, K. D., Zhao, W. et al., 1996. Partially molten middle crust beneath southern Tibet: Synthesis of project Indepth results. Science, 274, 1684–1688.

Pandey, S., Yuan, X., Debayle, E., Priestley, K., Kind, R., Tilmann, F., Li, X., 2014. A 3-D shear- wave velocity model of the upper mantle beneath China and the surrounding areas. Tectonophysics 633, 193–210. http://dx.doi.org/10.1016/j.tecto.2014.07.011.

Shen, XZ., Zhou, YZ., Zhang, YS., Mei, XP., Guo, X., Liu, XZ., Qin, MZ., Wei, CX., Li, CQ., 2014. Receiver function structures beneath the deep large faults in the northeastern margin of the Tibetan Plateau. Tectonophysics 610, 63-73.

Shen, XZ., Yuan, X., Liu, M, 2015. Is the Asian lithosphere underthrusting beneath the northeastern Tibetan Plateau? Insights from seismic receiver functions. Earth Planet. Sci. Lett. 428, 172-180.

Shi, D., Zhao, W., Klemperer, S., Wu, Z., 2016. West–east transition from underplating to steep subduction in the India-Tibet collision zone revealed by receiver-function profiles. Earth Planet. Sci. Lett. 452, 171–177.

Sippl, C.,Kumar, A., Dettmer, J., 2017. A cross-correlation based to direct seismogram stacking for receiver-side structural inversion. Bull. Seismol. Soc. Am. 107, 3, 1545-1550.

Sodoudi, F., Yuan, X., Liu, Q., Kind, R., Chen, J., 2006. Lithospheric thickness beneath the Dabie Shan, central eastern China from S receiver functions. Geophys. J. Int. 166:1363–67.

Sodoudi, F., Yuan, X., Kind, R., Lebedev, S., Adam, J.M.C., Kästle, E., Tilmann, F., 2013. Seismic evidence for stratification in composition and anisotropic fabric within the thick lithosphere of Kalahari Craton. Geochem. Geophys. Geosyst., 14, 5393–5412.

Stammler, K., 1993. Seismichandler programmable multichannel data handler for interactive and automatic processing of seismological analyses. Computers & Geosciences 19 (2), 135-140.

Vinnik, L. P. & Romanowicz, B. A., 1991. Origin of precursors to teleseismic S waves, Bulletin of the Seismological Society of America, 81(4), 1216–1230.

Wilson, D. C., Angus, D., Ni, J. F. & Grand, S. P., 2006. Constraints on the interpretation of S-to-P receiver functions, Geophysical Journal International, 165(3), 969–980, https://doi.org/10.1111/j.1365-246X.2006.02981.x.

Xu, Q., Zhao, J., Pei, S., Liu, H., 2013. Imaging lithospheric structure of the eastern Himalayan syntaxis: New insights from receiver function analysis. J. Geophys. Res. Solid Earth, 118, 2323–2332.

Yang, H., Peng, H., Hu, J., 2017. The lithospheric structure beneath south-east Tibet revealed by P and S receiver functions. Journal of Asian Sci-ences 138, 62-71.

Ye, Z., Gao, R., li, QS., Zhang, HS., Shen, XZ., Liu, XZ., Gong, C., 2015. Seismic evidence for the North China plate underthrusting beneath northeastern Tibet and its implications for plateau growth. Earth Planet. Sci. Lett. 426, 109-117.

Zhang, Z., Yuan, X., Chen, Y., Tian, X., Kind, R., Li, X., Teng, J., 2010. Seis-mic signature of the collision between the east Tibetan escape flow and the Sichuan Basin. Earth Planet. sci. Lett. 292, 254-264.

Zhao, J., Yuan, X., Liu, H., Kumar, P., Pei, S., Kind, R., Zhang, Z., Teng, J., Ding, L., Gao, X., Xu, Q., Wang, W., 2010. The boundary between the Indian and Asian tectonic plates below Tibet. PNAS 107, 25, 11229-11233.

Zheng, X.F., Yao, Z.X., Liang, J.H., Zheng, J., 2010. The role played and opportunities provided by IGP DMC of China National Seismic Network in Wenchuan Earthquake disaster relief and researches. Bull. Seism. Soc. Am. 100, 5B, 2866-2872.

Zheng, Y.-F., Xiao, W.-J., Zhao, G., 2013. Introduction to tectonics of China. Gondwana Res. 23, 1189–1206.

Figure Captions

Fig.1: Simplified tectonic map of China showing the major cratonic blocks (Zheng et al., 2013): NCC = North China Craton and SCB = South China Block. Inverted triangles mark location of permanent seismic broadband stations. Epicenters of the seismic events used are marked in the inlet.

Fig.2: Comparison of data processing results obtained with the new onset method (A) and the traditional S-receiver function method (B) along two east-west profile through the North China Craton. The width of the profiles is marked by the two red lines. Blue signals result from a discontinuity with velocity increase downward and red signal from a velocity decrease. Moho and lithosphere-asthenosphere boundary (LAB) are marked by dashed and solid lines, respectively in A and B. Note that the positions where depth data should be taken from profiles in A and B are different, since the definition of reference times is different in both methods. In the onset method measurements should be taken at the deepest (earliest in the time domain) part of the signal and in the S-receiver function method at the center of the signal. The LAB in B (S-receiver

function method) is continuous over the entire profiles whereas the LAB in A (new onset method) is disrupted and sharply deepening at the western edge of the North China Craton. This signal is probably overwhelmed by sidelobes in the deconvolution method.

Fig.3: Same as in Fig.2 for profiles located in the South China Craton. The dipping LAB from Fig.2A is barely visible (see question mark). Shallowing of the Moho at the easter edge of the South China Craton is observed in both methods marked by a Z in A (right panel). Conversions from the 410 km discontinuity and a negative discontinuity above the 410 km discontinuity are marked by 410 and LVL, respectively.

Fig.4: Two north-south profiles through the eastern parts of the North and South China Cratons. The LAB is clearly observed in both cratons near 80 km depth. In the profile along the coast (A) is in addition marked a structure Y which could be the Philippine plate subduction north of Taiwan.

Fig.5: A north-south profile through the eastern parts of the South and North China Cratons is shown in A. The dipping LAB structure is visible like in Figs.2A-3A. A north-west to south-east running profile is shown in B which shows the dipping LAB more clearly

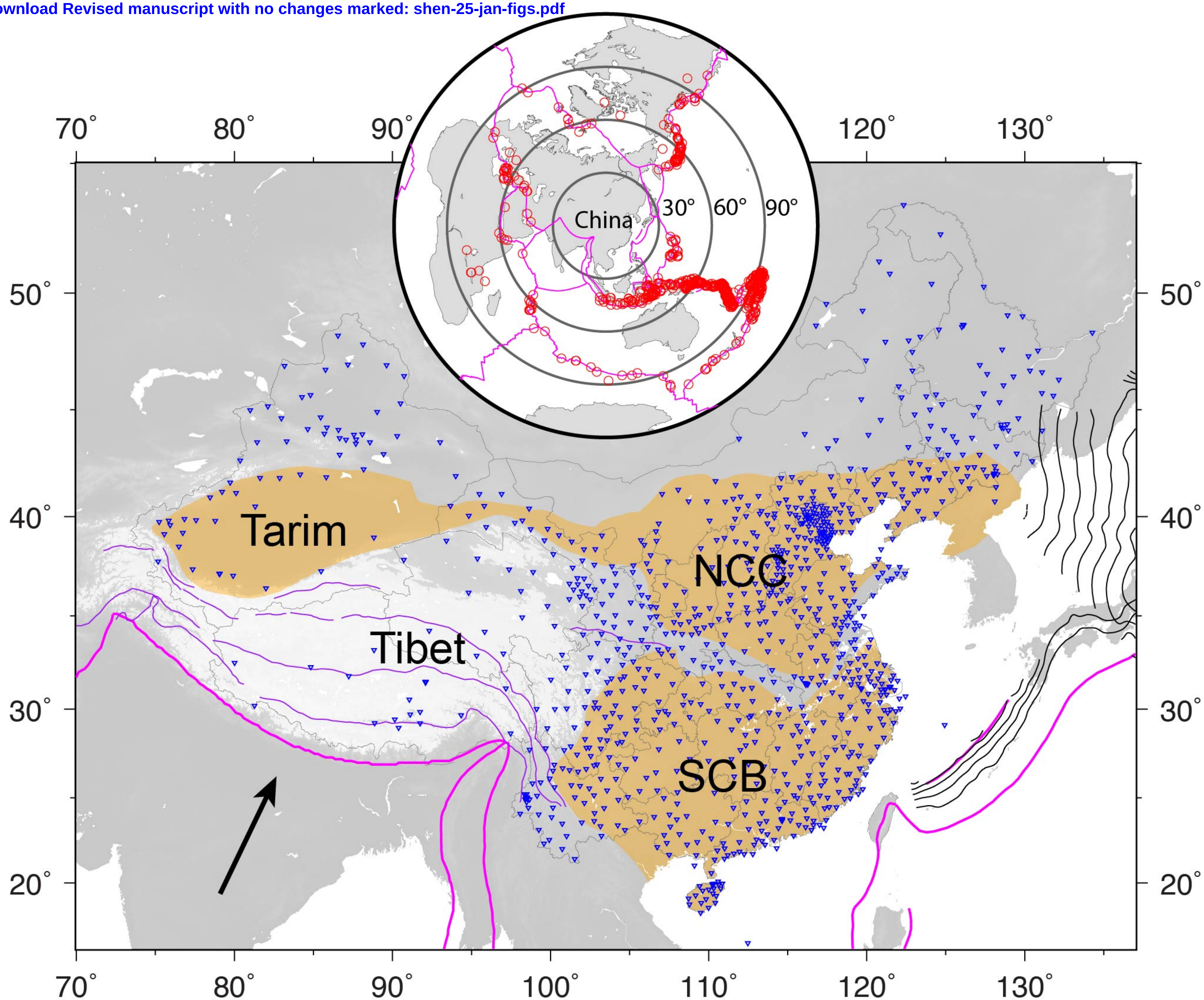
China
30°
60°
90°
Tarim
Tibet
NCC
SCB
70°
80°
90°
100°
110°
120°
130°
20°
30°
40°
50°

1

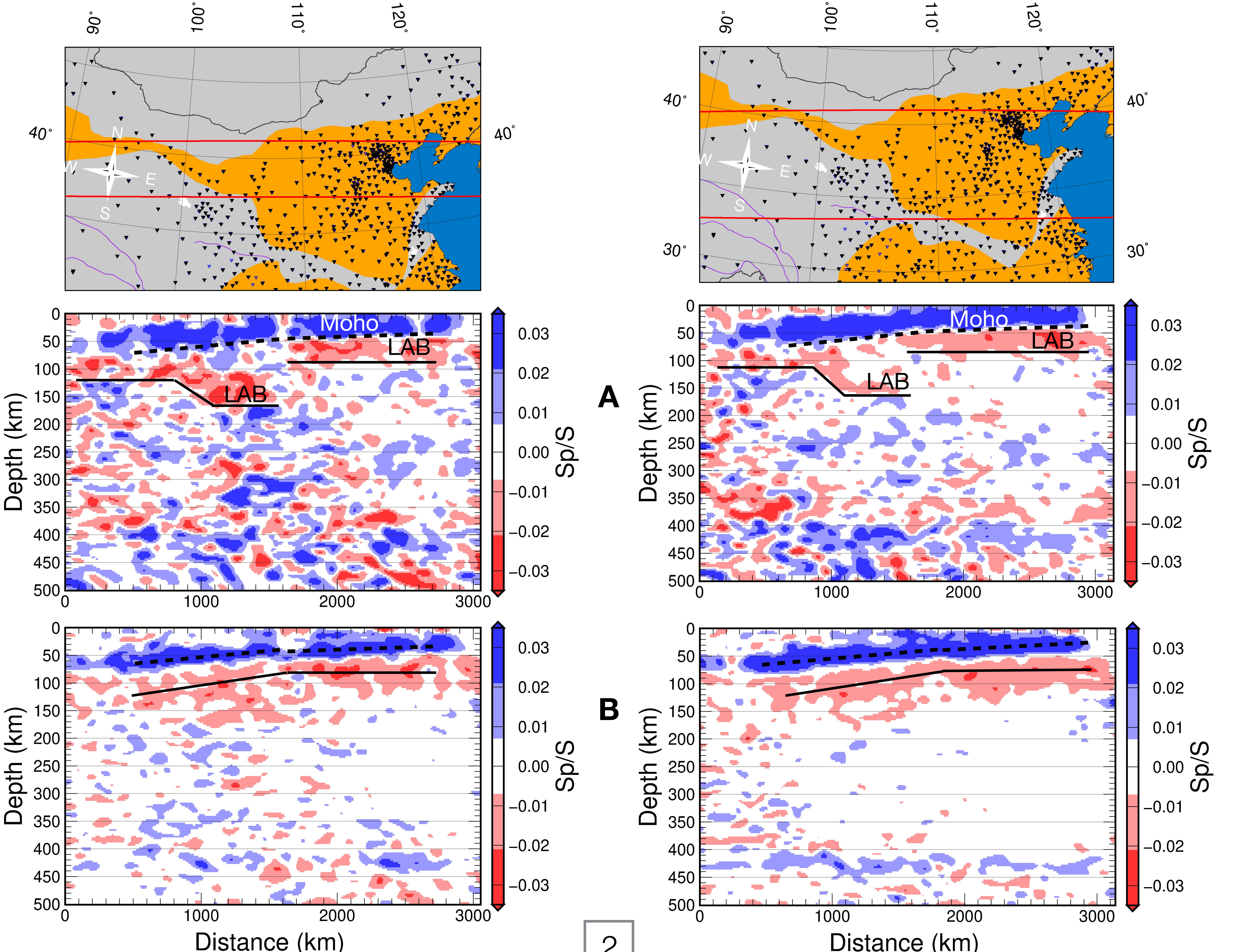
90°
100°
110°
120°
40°
30°
N
S
E
W
Moho
LAB
A
B
Depth (km)
Distance (km)
Sp/S
0.03
0.02
0.01
0.00
−0.01
−0.02
−0.03

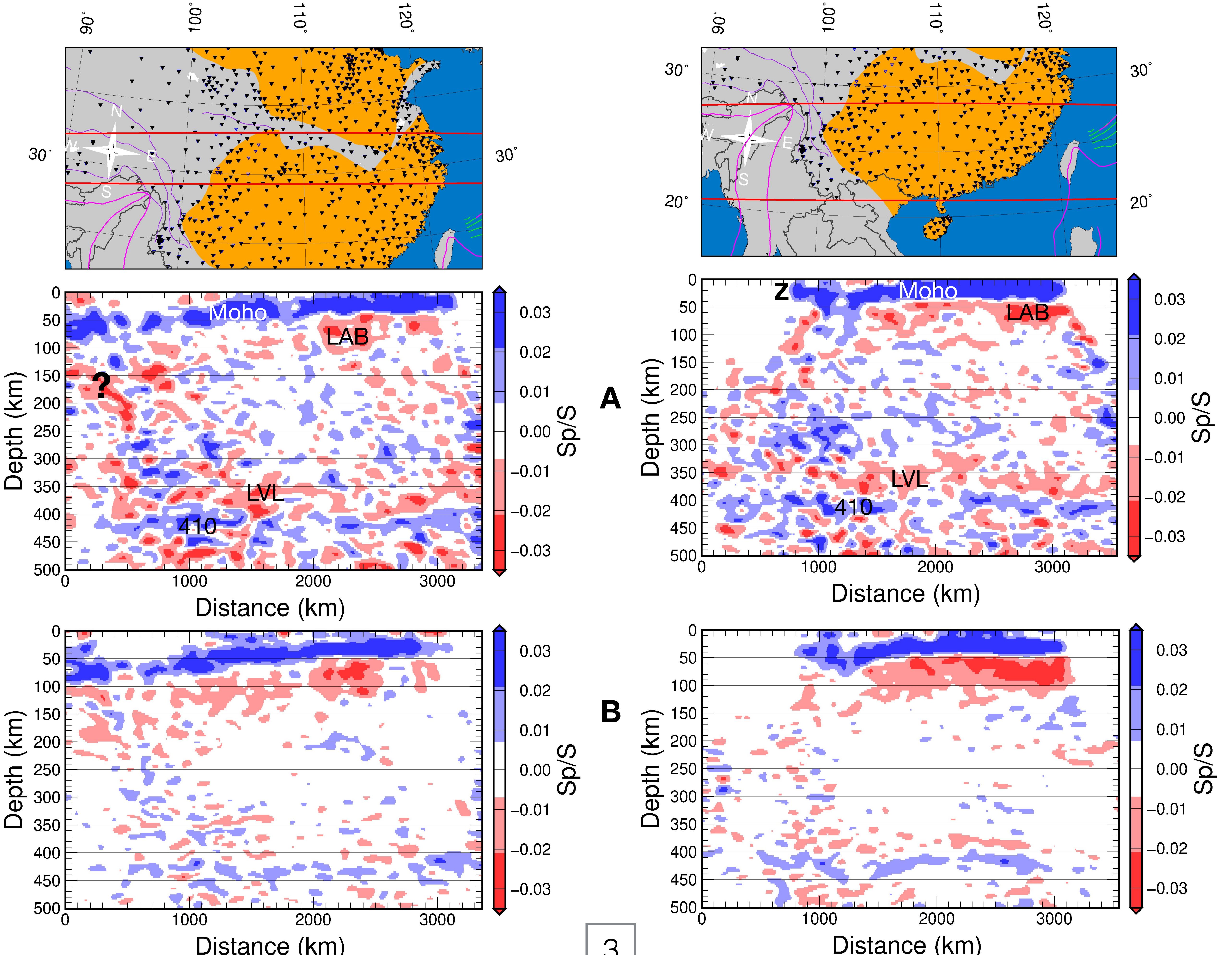
90°
100°
110°
120°
30°
20°
N
S
E
W
Moho
LAB
LVL
410
?
Z
A
B
Depth (km)
Distance (km)
Sp/S
0.03
0.02
0.01
0.00
−0.01
−0.02
−0.03

3

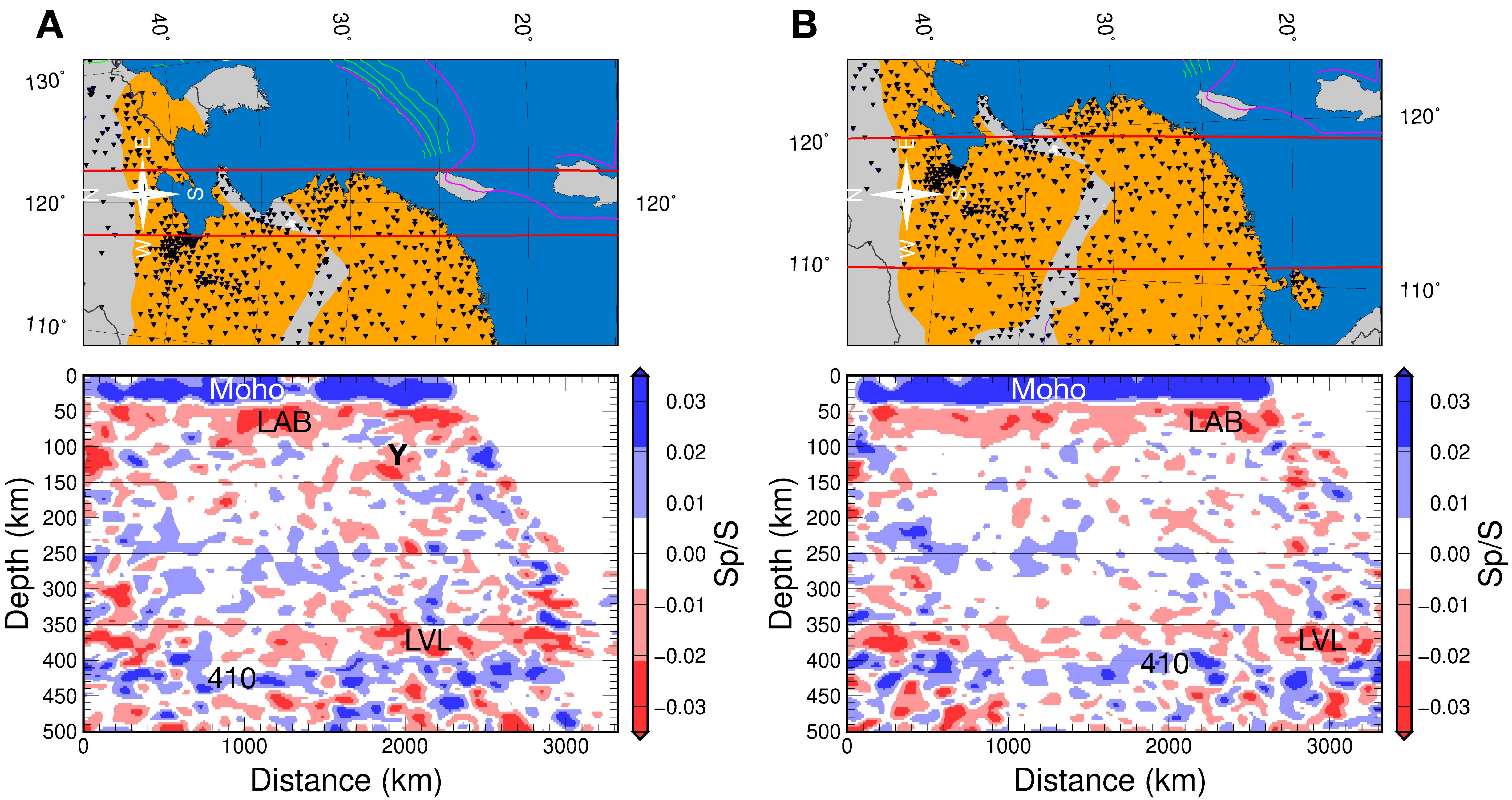
A
B
40°
30°
20°
130°
120°
110°
N
S
E
W
Moho
LAB
Y
LVL
410
Depth (km)
Distance (km)
0
50
100
150
200
250
300
350
400
450
500
1000
2000
3000
0.03
0.02
0.01
0.00
−0.01
−0.02
−0.03
Sp/S

4

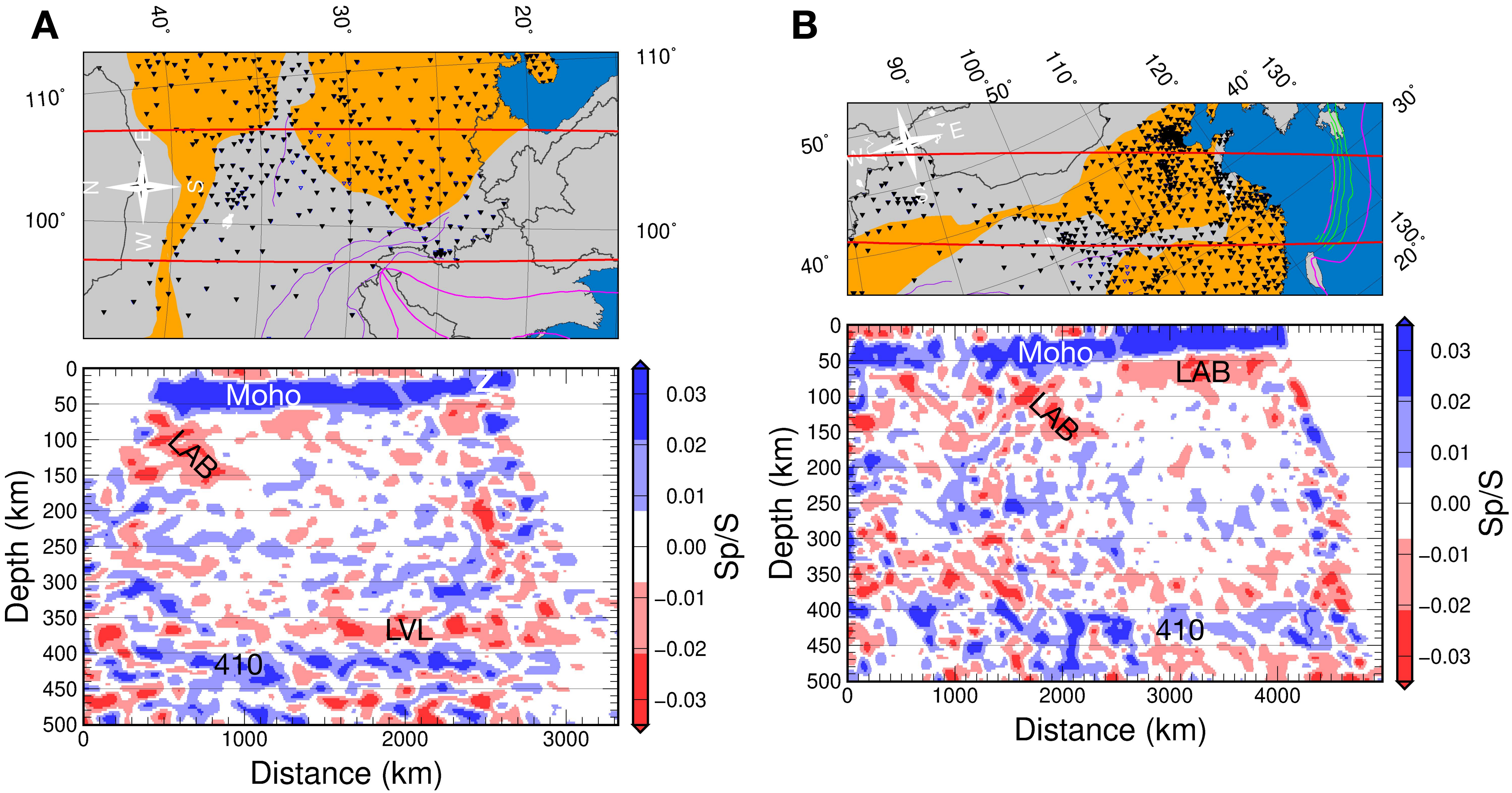
A
40°
30°
20°
110°
100°
Moho
LAB
LVL
410
Depth (km)
Distance (km)
Sp/S
B
90°
100°
110°
120°
130°
50°
40°
30°
20°
Moho
LAB
LAB
410
Depth (km)
Distance (km)
Sp/S